Measurement of the proton Gerasimov-Drell-Hearn integral at low Q^2.

December 2, 2002

A Hall A collaboration proposal

P. Bertin, A. Camsonne, H. Fonvieille, G. Laveissiere
Université Blaise Pascal/LPC, France

D. Margaziotis
California State University, Los Angeles

J. Yuan, S. Zhou
China Institute of Atomic Energy

D. Lhuillier
DSM/DAPNIA/SPhN CEA Saclay , France

R. De Leo, L. La gamba
INFN Bari, Italy

F. Cusanno, S. Frullani, F. Garibaldi, G. M. Urciuoli, M. Iodice
INFN/Sanita, Roma, Italy

E. Voutier
Institut des Sciences Nucleaires, Grenoble, France

J.P. Chen (co-spokesperson), D. Higinbotham, M. Jones, B. Reitz, Y. Roblin
Jefferson Lab, Newport News, VA 23606

P.E.C. Markowitz
Florida International University, Miami FL, 33199

S. Širca
Dept. of Physics, Univ. of Ljubljana, Slovenia

L. Kaufman, K. Kumar, K. Paschke
University of Massachusetts, Amherst, MA

B. Bertozzi, O. Gayou, S. Gilad, B. Ma, P. Monaghan, X. Zheng
Massachusetts Institute of Technology, Cambridge, MA 02139

C. E. Hyde-Wright

Old Dominion University Norfolk VA 23529

R. Gilman, X. Jiang, K. McCormick
Rutgers University, Piscataway, NJ 08855

T. Ruan, J. Shen, Y. Ye, Z. Yin, Yunxiu Ye
University of Science and Technology of China

Seonho Choi, Z.-E. Mezziani, K. Slifer, P. Solvignon
Temple University, Philadelphia, PA 19122

G. Cates, D. Crabb (co-spokesperson), D. Day, A. Deur (co-spokesperson and contact person)
B. Humensky, R. Lindgren, B. Norum, Y. Prok, O. A. Rondon, J. Singh
N. Liyanage, P. McKee. A. Tobias, R. Snyder, K. Wang, F. Wesselmann, H. Zhu
University of Virginia, Charlottesville, VA 22901

D. Armstrong, T. Averett, M. Finn, K. Kramer, K. Griffioen, V. Sulkovsky
The College of William&Mary, Williamsburg, VA 23185

Abstract

We propose to perform a high precision measurement of the Gerasimov-Drell-Hearn integral in the $0.015<Q^2<0.4$ GeV^2 range, using the Hall A High Resolution Spectrometers combined with the septum magnets. Such data will provide a clean benchmark measurement for Chiral Perturbation Theory and will help to disentangle theoretical issues related to χPT calculations. The combination of these proton data with neutron data will also be extremely valuable. Finally such a measurement will complete the proton data already taken at JLAB and in other high energy facilities in such a way that we will have measurements of the GDH integral on the proton in the full Q^2 range, i.e from the photon point to well into the DIS domain. We plan to use the UVa polarized NH_3 target. With 20 days of beam time we can reach a $\pm 2\%$ (stat) $\pm 8\%$ (syst) on the integral and ± 6 % (stat) $\pm 8\%$ (syst) on the spin structure function g_1.

1 Introduction

We present here a proposal for measuring the proton Gerasimov-Drell-Hearn integral (GDH) at low Q^2. We will first define the GDH sum rule and briefly recall its derivation and its theoretical basis. After a short review of its experimental status we will present the extension of the GDH integral at finite Q^2. Then we will discuss the interests of such a measurement at low Q^2, namely to complete the Q^2 range of the experimental measurements of the extended GDH integral and to provide a clean benchmark measurement for Chiral Perturbation Theory (χPT). In particular, this will help to disentangle theoretical issues with χPT calculations. The importance of combining proton data (this proposal) and neutron data (the approved experiment E97-110) will be pointed out. We will then detail the experimental aspects of such a measurement. We will end this document by giving the proposed measurement and the beam time estimate necessary to meet our goal.

1.1 The Gerasimov-Drell-Hearn sum rule

The original GDH sum rule has been derived [1] at Q^2=0. For spin 1/2 targets it reads

$$\int_{\nu_0}^{\infty} \sigma^{1/2} - \sigma^{3/2} \frac{d\nu}{\nu} = -2\pi^2 \alpha \frac{\kappa^2}{M^2} \qquad (1)$$

where $\sigma^{1/2}$ ($\sigma^{3/2}$) is the polarized photoproduction cross section when the photon helicity is anti-aligned (aligned) with the target spin. ν_0 is the pion photoproduction threshold, ν the photon energy, κ the anomalous magnetic moment of the target and M its mass. Anticipating the generalization of the sum rule at finite Q^2, we relate the transverse-transverse interference cross section to the polarized photoproduction cross sections

$$\sigma^{TT} = \left(\sigma^{1/2} - \sigma^{3/2}\right)/2$$

The sum rule derivation follows three steps:

1. A non-subtracted dispersion relation is used to link the real part of the forward Compton amplitude to the integral of the imaginary part, weighted by the photon energy. This assumes causality of the forward Compton amplitude.

2. The optical theorem expresses the imaginary part of the forward Compton amplitude in term of σ^{TT}. The optical theorem rests on unitarity.

3. A Low Energy Theorem expands the real part of the forward Compton amplitude in series of ν. The Low Energy Theorem assumes relativity and gauge invariance.

We can see that the derivation is based on solid theoretical grounds. The only assumption that might be open to questions is in step 1: The validity of the

non-subtraction hypothesis (absence of contribution from the circular contour when one performs the Cauchy integration to derive the dispersion relation). Convergence of the integral has been questioned. However, experimental data as well as theoretical bounds suggest that this hypothesis is correct [2].

1.2 Experimental Status

The GDH sum rule is thus a fundamental quantity and its relation has been used in analysis or theoretical predictions. It is then important to provide experimental checks. Another reason for experimental verifications of the sum rule is that the first indirect estimates [3] of the GDH integral, using single-pion photoproduction, have shown that the sum rule is violated. However, it is not clear whether the violation is real or comes from the limitation of using unpolarized and singly polarized pion data to perform this indirect estimate.

A dedicated check of the sum rule has been undertaken at the MAMI ($0.14<\nu<0.80$ GeV) and ELSA ($0.7<\nu<3.0$ GeV) facilities. The MAMI proton data [4] together with the ELSA preliminary analysis up to ν=2.8 GeV [5] show an over-saturation of the sum rule []. Clearly, in spite of the $1/\nu$ weighting, data at higher photon energy is needed for a complete check of the sum rule (SLAC E159 will take data on the proton for $5<\nu<40$ GeV [9]). Other facilities have undertaken measurement of the GDH integral (GRAAL [7], JLAB [27] LEGS [8], SLAC [9], Spring8 [10] and TUNL [11]).

1.3 The Extended GDH Sum Rule

Anselmino et al [12] suggested that the GDH integral extended to finite Q^2 will help to understand the transition from perturbative to non-perturbative QCD. The connection between the extended GDH integral and the Bjorken integral was also pointed out. The generalization consists of replacing the photoproduction cross sections by the electroproduction ones (for a review, see [13]). Different generalizations exist depending on the choices of the convention for the virtual photon flux and on the way the spin structure function g_2 is included.

Among these different GDH extensions, the one of Ji and Osborn [14] stands out because it generalizes not only the integral side but the full sum rule. Hence it keeps the checking power of a sum rule that was lost with the former definitions. In addition Ji and Osborn showed that the Bjorken and the GDH sum rules are different aspects of their generalized GDH sum rule. It is written

$$4\int_{\nu_0}^{\infty} G_{1(2)}\frac{d\nu}{v} = \overline{S_{1(2)}} \qquad \text{(eq. 2)}$$

where $G_{1(2)}$ are the spin structure functions of the nucleon and $\overline{S_{1(2)}}$ are the forward Compton amplitudes with the elastic contribution subtracted. $G_{1(2)}$ are related to $g_{1(2)}$

$$g_1(x,Q^2) = \frac{\nu}{M^2}G_1(\nu,Q^2)$$
$$g_2(x,Q^2) = \left(\frac{\nu}{M}\right)^2 G_2(\nu,Q^2)$$

The forward Compton amplitudes are presently calculable using chiral perturbation theory at low Q^2, higher twist expansion at larger Q^2. Eventually lattice QCD calculations will provide calculations at any Q^2. Let us note that moments of the spin structure function are quantities particularly well suited for lattice QCD calculations.

In this proposal we will use the following definition for the extended GDH integral

$$I(Q^2) = \frac{2M^2}{Q^2}\Gamma_1(Q^2) \qquad \text{(eq. 3)}$$

where $\Gamma_1(Q^2) \equiv \int g_1(Q^2,x)dx$ is the first moment of the spin structure function g_1.

CERN [15], SLAC [16] and HERMES [17] have provided data for $I(Q^2)$, mainly in the DIS regime, for both the proton and the neutron. Several experiments at Jefferson Lab have been or will be performed [21], [22], [23] to measure the extended GDH integral at low and intermediate Q^2 for the neutron and at intermediate Q^2 for the proton. The experimental results of Hall A and Hall B as well as Hermes are shown in the Figure 1.

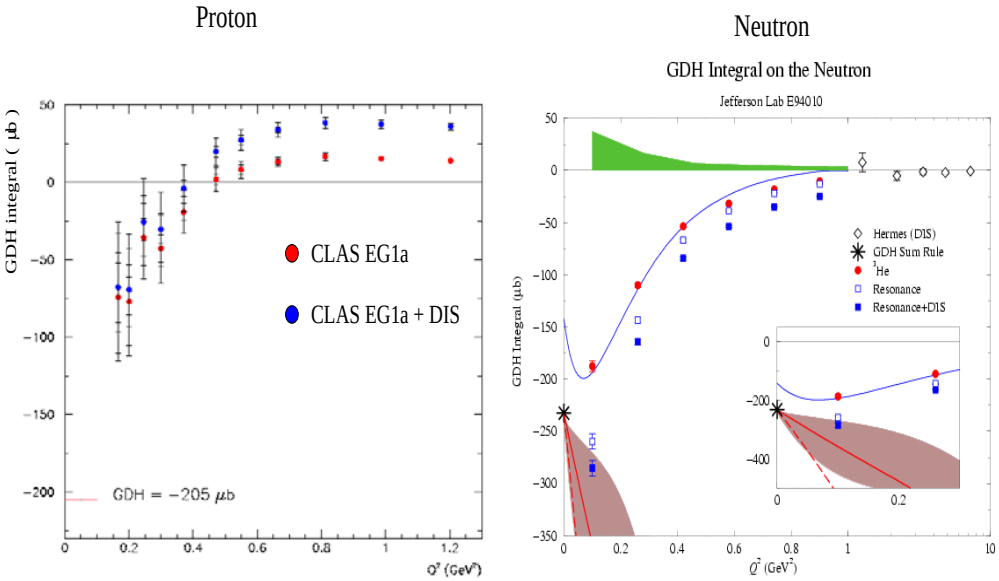

Fig. 1. Q^2 evolution of GDH(Q^2) on the proton and neutron.

1.4 Proposal

We propose to perform a high precision measurement of $I(Q^2)$ in the $0.015<Q^2<0.4$ GeV^2 range, using the Hall A High Resolution Spectrometers combined with the septum magnets. Such data complete the Q^2 coverage of the $I(Q^2)$ data on the proton. They will link the E91-023 (EG1) Hall B data to the real photon

GDH data from MAMI [4] and ELSA [5]. The low Q^2 part of the data will provide a benchmark measurement for Chiral Perturbation Theory. At higher Q^2, the overlap with the Hall B data will provide, in the important area of the zero-crossing, a valuable cross-check between two experiments using widely different detectors.

We propose to do this measurement in Hall A because it is the only Hall that can perform the forward angle measurements necessary to reach such low Q^2.

2 Motivations

2.1 Chiral Perturbation Theory (χPT)

2.1.1 Importance of the validation of χPT

The release of the JLAB results on GDH at intermediate Q^2 [21], [22] at the GDH2002 workshop [20] triggered discussions showing a large interest for doing an extension to smaller Q^2. The first goal of this experiment will be to provide benchmark data on the proton at low Q^2 to compare to χPT calculations (and later to Lattice QCD calculations).

χPT calculations are the only rigorous computations available presently for GDH(Q^2) at low Q^2 [18], [19]. There are several theoretical issues regarding the accuracy and domain of application of χPT:

- The convergence of the series: The next to leading order term being large (it changes the prediction of the slope of GDH(Q^2) at the photon point), it is not obvious that the first few terms are sufficient for establishing a reliable χPT prediction.
- The importance of inclusion of the resonances in χPT calculations.
- The Q^2 range of applicability of χPT.

Accurate data on both the proton and the neutron will provide constraints that will help to disentangle these issues.

2.1.2 Proton and Neutron

Since a neutron GDH experiment in the same Q^2 range is scheduled to run soon in Hall A (E97-110, [23]), it is legitimate to ask what further information does the proton bring.

The obvious answer is that a different nucleon provides additional data to constrain the theory. Furthermore, the proton has the advantage that its data, conversely to the neutron data, will not have the uncertainty due to the delicate extraction of the neutron information from the nuclear medium. However the most interesting point is the combined use of both nucleon data: GDH proton

data together with GDH neutron data are necessary to form the "Bjorken integral"[1] $I^{p-n}(Q^2)$=$I^p(Q^2)$−$I^n(Q^2)$. This quantity is also calculable in χPT and the range of applicability of the calculation is expected to be larger than for the GDH integral because the contribution of resonances mostly cancels out [24]. Its upper Q^2 range of applicability is expected to be close to the lower Q^2 range of applicability of the Higher Twist Expansion. If this is verified our proposed experiment, together with the E97-110 data, will allow for the first time to have a complete Q^2 coverage of the "Bjorken integral", the quantity which is the best suited for comparisons to the different calculations valid in the different regimes of QCD.

Finally, after extrapolation of the proton and neutron sum rules at the photon point, the Isoscalar, Isovector and Interference GDH sum rules [25], [26] can also be formed.

2.2 The original GDH Sum Rules

The original GDH Sum Rule (i.e. at the real photon point) on the proton $I^p(Q^2 = 0)$ is being checked at MAMI [4], ELSA [5], GRAAL [7], JLAB [27] LEGS [8], SLAC [9], Spring8 [10] and TUNL [11]. Measuring the original GDH sum rule by extrapolation from nearly real photon data would provide an independent cross-check using a different technique. Such an independent check with a sufficient integration range is very important since one cannot rely on only one result for the real GDH experiment. This is especially true knowing that the preliminary η' photoproduction data from Hall B seem to disagree with the ones from ELSA.

In combination with the neutron data, we can form the difference $I^p(Q^2)$-$I^n(Q^2)$ the value of which is predicted at the photon point by the GDH sum rules on the proton and the neutron. This is the best quantity to extrapolate to the photon point since its evolution is smoother than the individual $I^p(Q^2)$ and $I^n(Q^2)$ due to the partial cancellation of the resonance contribution.

3 Experimental Setup

The kinematic coverage and experimental setup, apart from the target, are similar to the ones of E97-110 [23]. The Q^2 coverage of the accepted $I(Q^2)$ experiment on the neutron at low Q^2 (E97-110 [23]) is shown in Fig. 2.

[1] Rigorously, the Bjorken sum rule is defined in the Bjorken limit. However the Operator Product Expansion is used to extend the sum rule to finite Q^2. This extended Bjorken sum rule is still just called the "Bjorken sum rule". We follow here this convention.

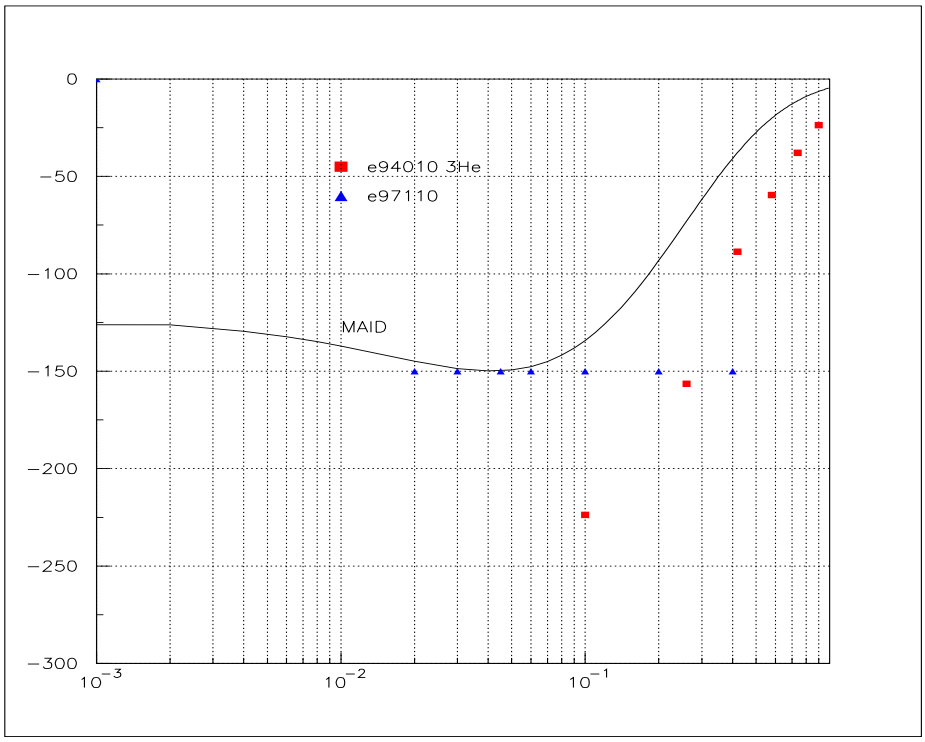

Fig. 2. Q^2 coverage of the experiment E97-110 on the neutron.

3.1 Spectrometers and data acquisition

We will use the 2 HRS of Hall A with their septum magnets. They will allow the detection of particles at 6^o and 9^o. Both spectrometers will be used for electron detection and set to symmetric setting. This will reduce and allow for a check of our systematic errors.

Since we are at forward angles, the maximal DAQ rate will often be the limiting quantity. In the time estimate below, we have taken a limit of 3 kHz for each arm, which is expected to be achieved for the up-coming E97-110 experiment.

As far as the spectrometers and data acquisition are concerned, there is no particular requirement for this experiment.

3.2 Beam Line

A polarized beam is required. In the time estimate below, we have assumed 80% polarization. The polarimetry will be provided by the Compton and Moller polarimeters.

The maximal beam current required will be about 0.10 μA in order to keep the target cool enough and minimize the depolarization process, see next section. Such a current is below the linear range of the Beam Current Monitor. To

monitor the charge, we plan to use the new silver calorimeter currently under development by the accelerator division. At such low current, new devices will also have to be installed to monitor the beam position. The pre-existing Hall C or Hall B Beam Position Monitors would be appropriate. All the changes on the beam line diagnostic devices will be the same as for Hall C with the improvement of the silver calorimeter. Hence there is no Research & Development issues with such a change.

3.3 Polarized proton target

We will use the UVa NH_3 polarized target that has been used in Hall C and SLAC. Let us note that we could also use the Hall B one but the implementation in Hall A will require more work.

3.3.1 Principle and description

A solid dynamically polarized proton target is proposed for this experiment. Dynamic nuclear polarization (DNP) is used to enhance the polarization of protons in $^{15}NH_3$. Polarizations above 95% have been already obtained. The target material is made up of frozen $^{15}NH_3$ granules of 1.0 mm to 3.5 mm in size which have been pre-irradiated in liquid argon with a 30-65 MeV electron beam. The ammonia is stored in liquid nitrogen when not used in the target apparatus. The main components of a polarized target are shown in Fig 3.

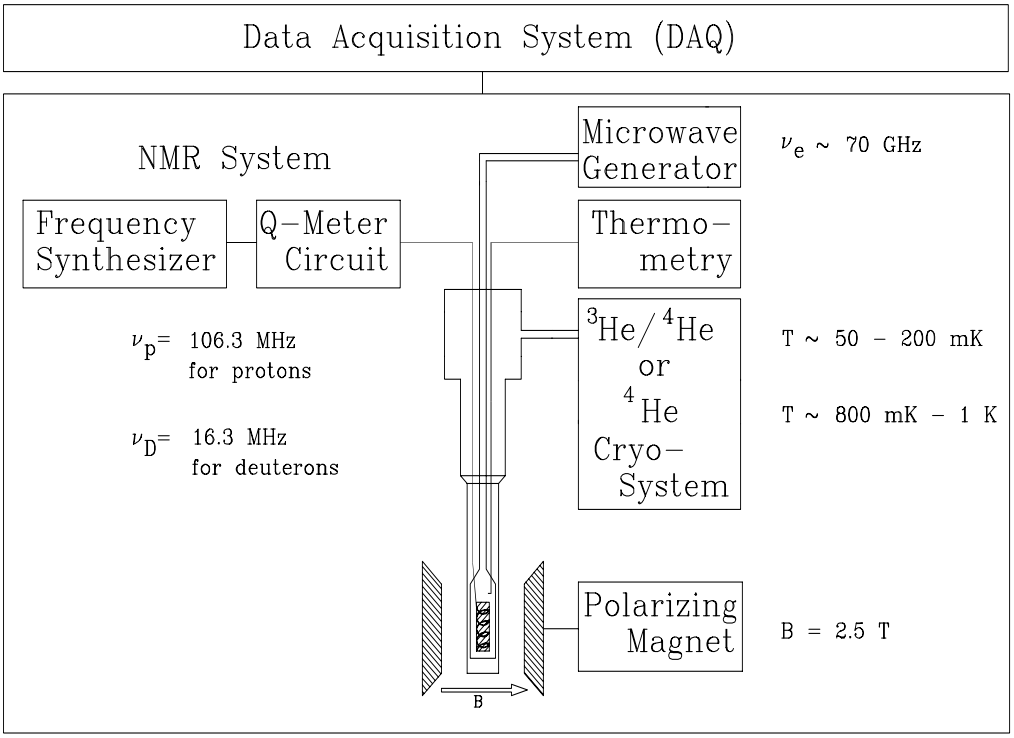

Fig. 3. A generic polarized target showing the major subsystems and typical operational parameters. Not shown are the standard vacuum and Roots pumping systems.

For DNP to work, a suitable material must be doped, either chemically or by irradiation, with paramagnetic centers that provide "free" electrons that can be manipulated. Then the material is placed in a high magnetic field and cooled to below 1K. Zeeman splitting and hyperfine splitting occur as shown in Fig 4. This is for the case of discrete energy levels (a crystal) and though most materials in use today are amorphous it illustrates the principle of DNP.

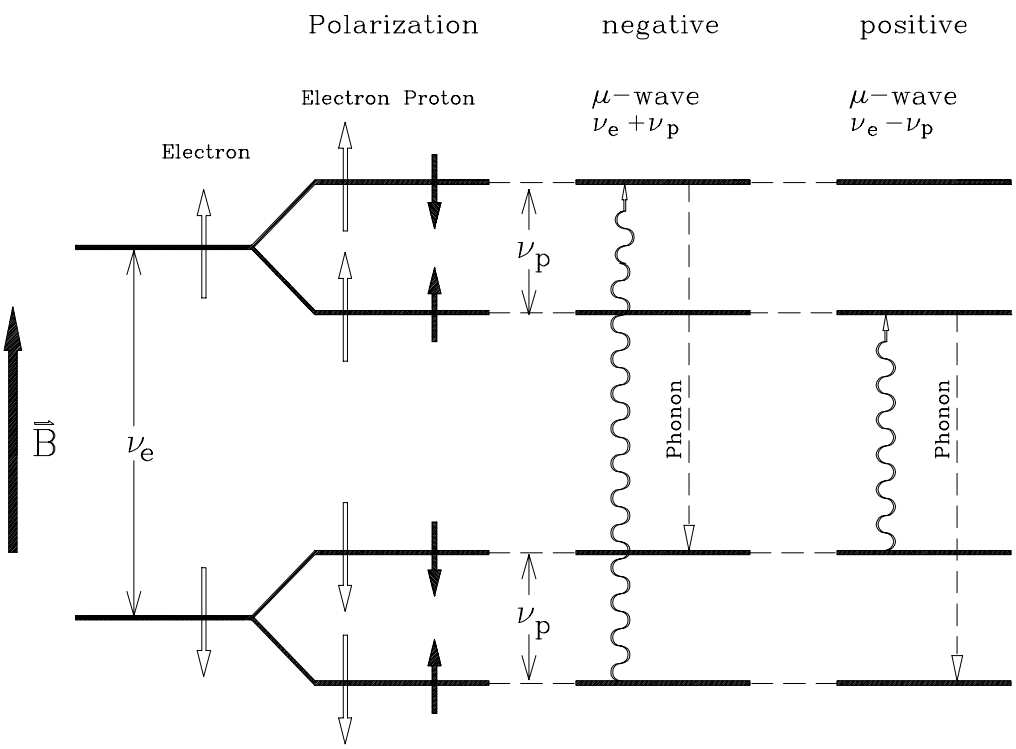

Fig. 4. Schematic of the resolved solid-state effect

Then if microwaves of a particular frequency are applied, the electron will flip from spin down to spin up and sometimes a proton will be flipped due to the hyperfine interaction. However the electron will relax to the lattice almost immediately ($\sim$ ms) and can be flipped again, while the proton can relax very slowly ($\sim$ hours) to the lattice, depending on the conditions. Thus the proton polarization can be built up. Another process is necessary to spread the polarization throughout the volume of the material - spin diffusion.- where the proton that has been flipped (usually very near the electron) will undergo the allowable flip-flop process with the surrounding protons, allowing a uniform polarization throughout the material.

DNP is achieved by way of a 5.1 Tesla Oxford Instruments superconducting Helmholtz pair magnet, a ^{4}He evaporation refrigerator that can reach temperatures below 1 Kelvin and a Varian extended interaction oscillator (EIO) tube that delivers 140 GHz microwaves to the target in order to drive the DNP process (figure 5).

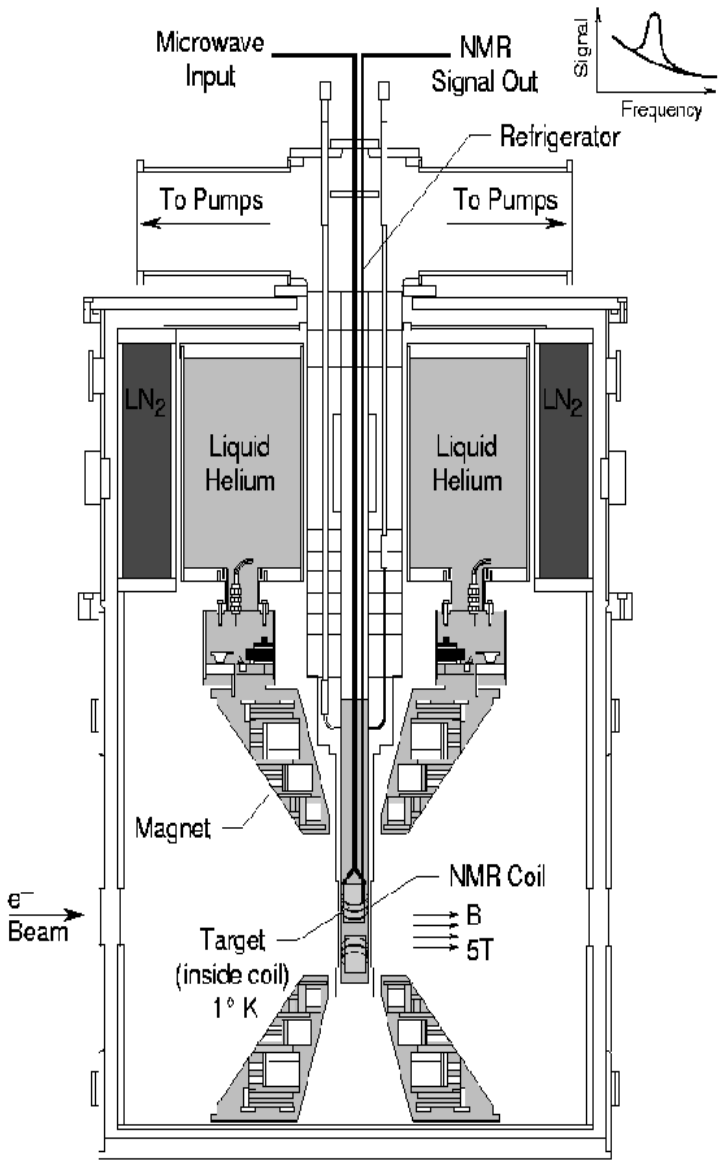

Fig.5 The target system as used at SLAC and JLAB Hall C

Five foot long inserts are used, each of which can hold various target cell configurations (figure 6). The target cells, which are fed by microwave horns, are used to hold and polarize the proton target material. CuNi tubing is used as the NMR coil material.

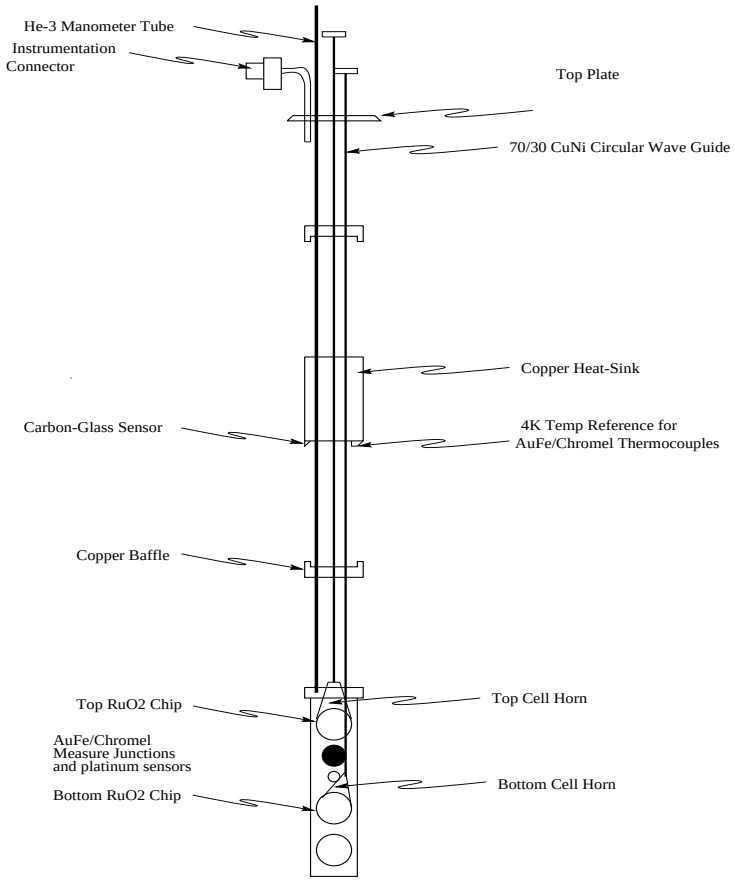

Fig. 6. Typical target ladder configuration as used in SLAC experiment E155.

An NMR system monitors the target polarization. It consists of Liverpool type Q-meters by way of a constant current series tune. The circuits were tuned to the corresponding Larmor frequency of the spin species being measured. In a 5.1 Tesla magnetic field and at 1 Kelvin temperature, the proton frequency is 213MHz. A frequency generator was swept through the resonance with the resulting signal area proportional to the nucleon polarization. Figure 7 shows the typical constant current series LCR circuit.

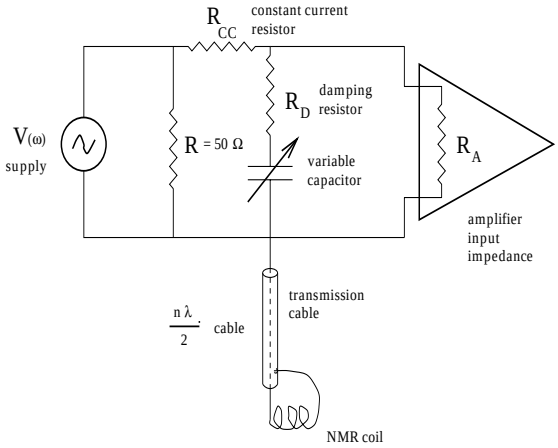

Fig. 7 Current Series LCR Circuit

This target has been used successfully at SLAC and in JLAB Hall C. Beside the interest for this proposal, extending the physics capabilities of Hall A will open possibilities for further experiments [32]. Since the target has already been installed in two experimental halls (Hall C and SLAC ESA) and since Hall A has the facility to run cryogenic targets, we do not foresee any difficulty related to the installation of the NH_3 target in Hall A.

3.3.2 Effect of the 5 Tesla field on the scattered electrons

The scattered electrons will be bent by the 5T target field. On the outgoing electron path, we have a $\int$Bdl=70 T.cm. If the field is anti-aligned with the beam direction, its effect will be to bend the electrons forward toward the beam line (c.f. Figs. 8 and 9 for simulation results). The field will also shift the vertical angle (in opposite directions for the left and right HRS).

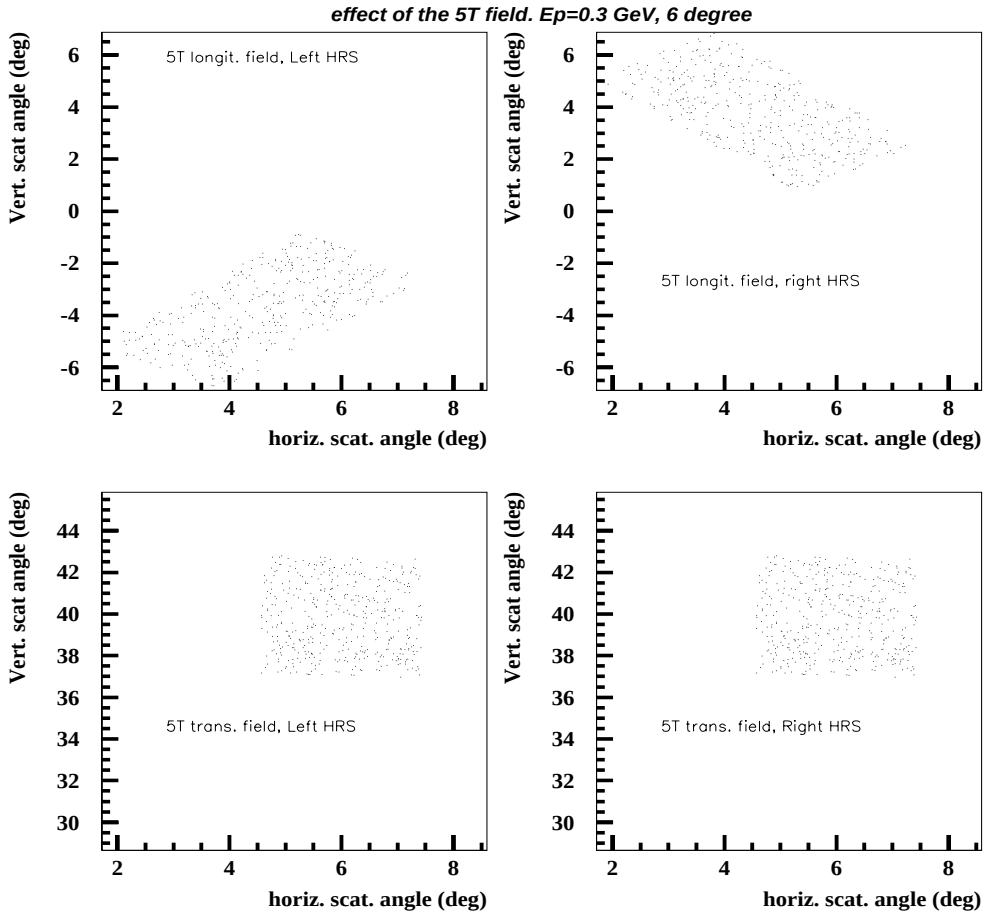

Fig. 8. Effect of the target field on the left and right spectrometer acceptances. The top plots show the distortion of the acceptance due to a 5T parallel field for a HRS momentum setting of 0.3 GeV (biggest effect). This gives the initial scattering angle of the electrons that reach the spectrometer focal plan. The bottom plots show the effects for a 5T transverse field. This is for a 6 degree HRS nominal setting.

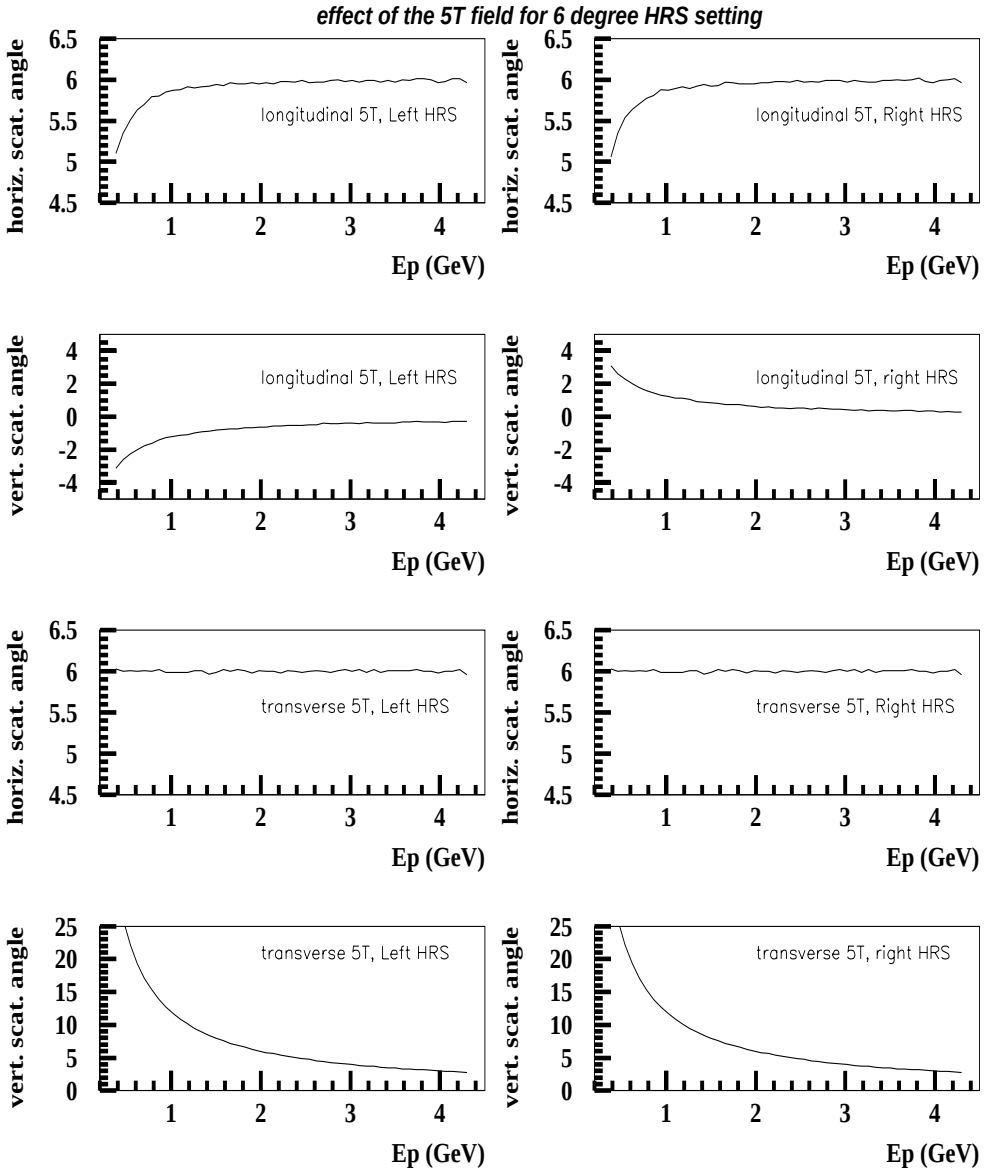

Fig. 9. Effect of the target field on the average scattering angle in function of the scattered electron energy (Ep), for a 6 degree HRS nominal setting. In this experiment, Ep will range from ∼0.4 GeV to ∼3.8 GeV. The four top plots are for a longitudinal field. The four bottom plots are for transverse.

For a longitudinal field, the effect on the detected angle is small in the range of the detected momentum ($\sim$0.4 GeV to $\sim$3.8 GeV). An anti-parallel field will make the low energy electrons from larger angles to be detected instead of the ones scattered at an angle corresponding the HRS angle setting. This will decrease the ν dependence of Q^2 at fixed beam energy. So this small effect is beneficial. For the same reason, the ratio between the inelastic rate and the elastic tail rate will also be improved, which is desirable for this experiment as we will see in section 3.3.3. It may seem desirable to use a parallel magnetic field to decrease the lowest Q^2 achievable. However, the field will act significantly only at large ν. Since an interpolation is needed in order to perform the integral at fixed Q^2 -this is discussed in section 6.1.1- and since the delta resonance is dominating the integral, the Q^2 value at which the interpolation is done is chosen close to the data on the delta where the Q^2 lowering effect of the field is not significant. As a consequence, using a parallel field would not lower the kinematics coverage of the experiment and would just increase the systematic error at large ν due to the interpolation. Furthermore, it would decrease the ν integration range of $I(Q^2)$ since the elastic tails will rise faster. Hence it is more desirable to use a antiparallel magnetic field for this experiment.

The transverse field that would be necessary for transverse data taking has a significant effect and will forbid detection at low momentum due to the decrease in counting rate (at E'=0.3 GeV, the electrons detected in the HRS has an initial vertical scattering angle of $\sim 40^o$). For the same reason, the coverage the low Q^2 kinematics where E$\sim$1-2 GeV is problematic. However, the absence of transverse data is not a limitation for this experiment as it will be shown in section 4.

3.3.3 Radiation lengths

Because of the forward angle detection, the elastic radiative tails are large and become a limitation for this experiment. The radiation lengths in the electron's path has to be minimized. In this proposal, we take the same materials as for the Hall C E93-026 G_e^n experiment but replacing the Al windows in the beam path by Be windows and removing the NMR coils from inside the cell.

The dominant radiation length is coming from the $^{15}NH_3$ cell itself. Fortunately, the tails are large only at low beam energy (see plots in the appendix). Here we will be limited by the maximal DAQ rate (3 kHz) and long cells are not necessary. We have computed that reducing the size of the cell down to 0.5 cm or 1 cm will allow to take reasonable data down to E=1 GeV. At larger beam energies or low ν, one can switch back to the regular 3 cm cells.

Let us note that the 5T field effect will improve the ratio between the inelastic rate and the tails.

3.3.4 Raster and cell diameter

Issue and considered solution The polarimetry pick up coil will measure the average polarization of the cell. However the relevant polarization value is at the region where the beam interacts with the cell; a non-uniform polarization

distribution within the cell would induce a bias. In order to have a uniform polarization, the cell has to be uniformly illuminated with the beam. This requires the triangular raster and a raster size equal to the cell diameter. Due to the aperture limitation of the Hall A beam line, the current raster size cannot be larger than 1 cm (given that we leave safety room for the beam transport). A modification of the beam pipe is necessary in order to accommodate for a raster diameter of the size of the cell. Only the pipe after the last Hall A quadrupole has to be replaced, which is a relatively minor task. Given the geometry of the beam pipe, the openings of the quadrupoles and the envelope of the beam, a larger beam pipe after the quadrupole will permit to achieve a sufficiently large raster size [31].

Alternative solutions Another solution would be to use 1 cm diameter cells instead of the 2.54 cm diameter cell currently used. We limit the maximum current to be put on the cells to 70 nA. The depolarization of a cell due to radiation damage follows $P = P_{max}e^{-I/I_0}$ with $I_0 \simeq 1 \times 10^{16}$ particles/cm^{-2}. To recover a larger polarization, the cells have to be annealed. This procedure takes about one hour. It will take about 2 hours at 70 nA to degrade the polarization from 95% to 65%. Since the diameter of the cell will be smaller than the current diameter, we can have up to 6 cells on the target insert. This implies that we have to anneal the target twice per day for the lowest rate kinematics. Annealing the target may also be done during some of the overhead times. The microwave has to be directed only on the cell in use so that the other cells are not polarized. This will avoid the contamination of the NMR signal from the signals due to the polarization of the other cells. The overhead time due to the build up of the polarization after each cell switch (15-20 min) and the modifications of the target ladder and vacuum chamber make this solution less attractive than a modification of the beam pipe.

Another solution would be to use lithium hydrate instead of ammonia since the former is less sensitive to radiation damage. However the dilution is larger with lithium and the maximum polarization reached with lithium hydrate material is significantly less than with ammonia (70% vs 95%).

4 Transverse data

Transverse data taking requires the installation of a chicane in order to bend back the beam into the beam dump. The maximal deviation (1 GeV beam) would be 6^o. We could also use a new beam dump able to handle 100 nA of beam current . Since the installation of the chicane or a beam dump is a significant effort, it is legitimate to question the importance of transverse data taking for GDH at forward angles. We address this point here.

We have seen that we can define the GDH integral with $\Gamma_1(Q^2)$, the first moment of the spin structure function g_1 (eq. 3). This is essentially a longitudinal quantity. The Fig. 10 shows a simulation of $g_1(\nu)$ at Q^2=0.1 GeV^2 from MAID and the error coming from the use of a model for the transverse data. To

establish the uncertainty due to the model, we also used MAID for generating $g_2(\nu)$ and varied it by +/- 100%. We see little dependence of $\Gamma_1(Q^2)$ with the transverse model (less than 5%). Hence an accurate measurement of $\Gamma_1(Q^2)$, at small angle will not require transverse data.

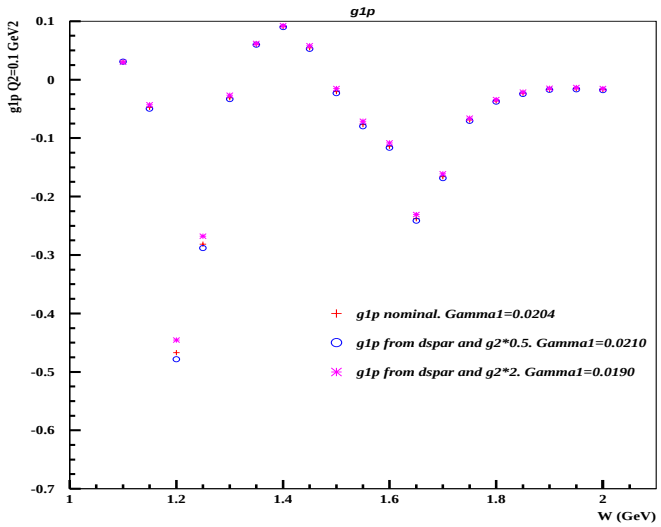

Fig. 10. $g_1(Q^2 = 0.1, W)$ for the proton at Q^2=0.1 GeV^2. $g_2(\nu)$ from MAID has been varied by +/- 100% to check the model dependence of $\Gamma_1(Q^2)$.

The preliminary results [21] of the experiment E94-010 indicate that the Maid model is reasonable (see Fig. 11) and that the previous assumption of having a model with a 100% uncertainty is more than conservative. The larger width of the resonance peak for the experimental data is due to the Fermi motion of the neutron within the ^{3}He nucleus.

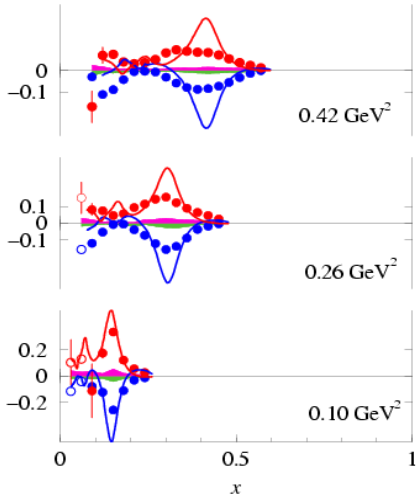

Fig. 11. $g_1^{^3He}$ (blue dots) and $g_2^{^3He}$ (red dots) from E94-010 (preliminary) and compared to the Maid model for g_1^n and g_2^n. The smearing of the ^{3}He data is due to the Fermi motion. The relevant quantities to compare are the areas below the experimental data and the Maid prediction.

4.1 Conclusion

The uncertainty from a modeled g_2 on the first moment $\Gamma_1(Q^2)$, or similarly on the generalized GDH integral, see eq. 3, is small: a 100% uncertainty on the model will propagate to a 6 to 7 % uncertainty on Γ_1. The modification of the beam line to accommodate transverse data taking requires a significant work. As a consequence, we propose to measure only longitudinal quantities.

5 Installation

The polarized target has been installed twice at SLAC (experiments E143, E155) and several time in JLAB Hall C (two runs of experiment, E93-026, experiment E01-006). Also the system has been set up several times in test areas at both labs and UVA. Given this experience and the cryogenic capacities of Hall A that already run a 600 W cryotarget, no difficulties for the installation in Hall A are foreseen. The target fits well in Hall A, see Fig. 12, 13 and 14. No modification of the scattering chamber will be necessary. The target support has to be adapted to Hall A and the scattering chamber has to be connected to the septum magnets. Both tasks are minor.

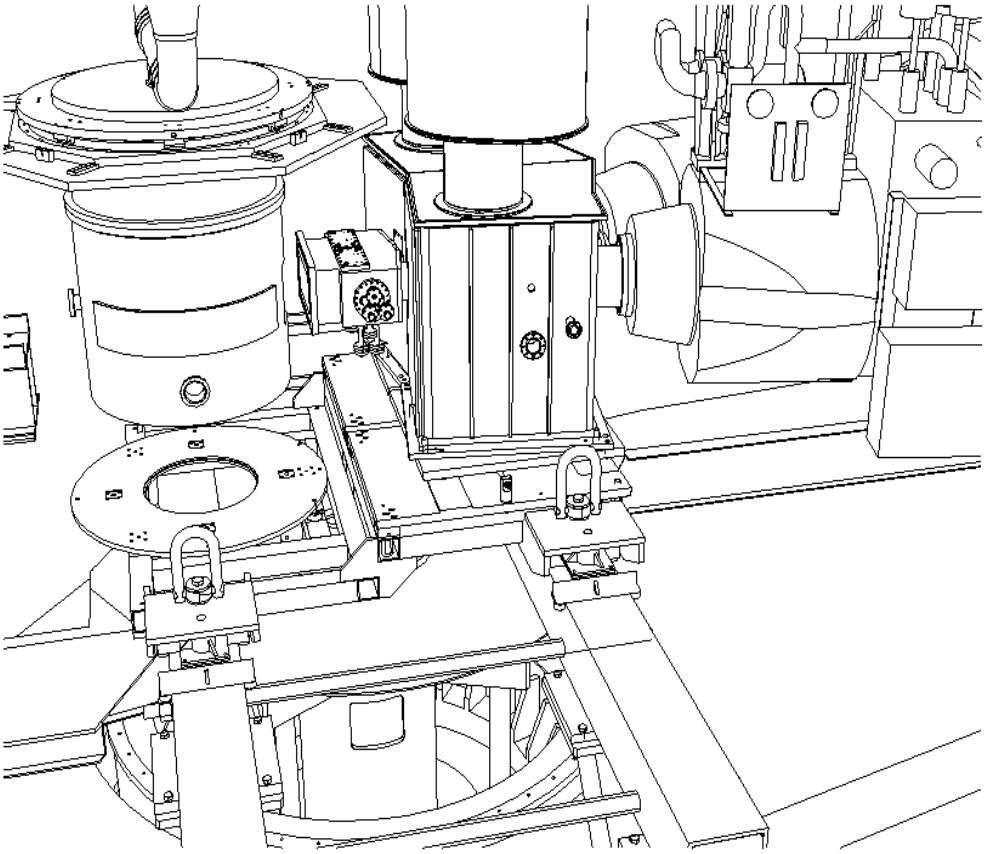

Fig. 12 The target in Hall A. Perspective view.

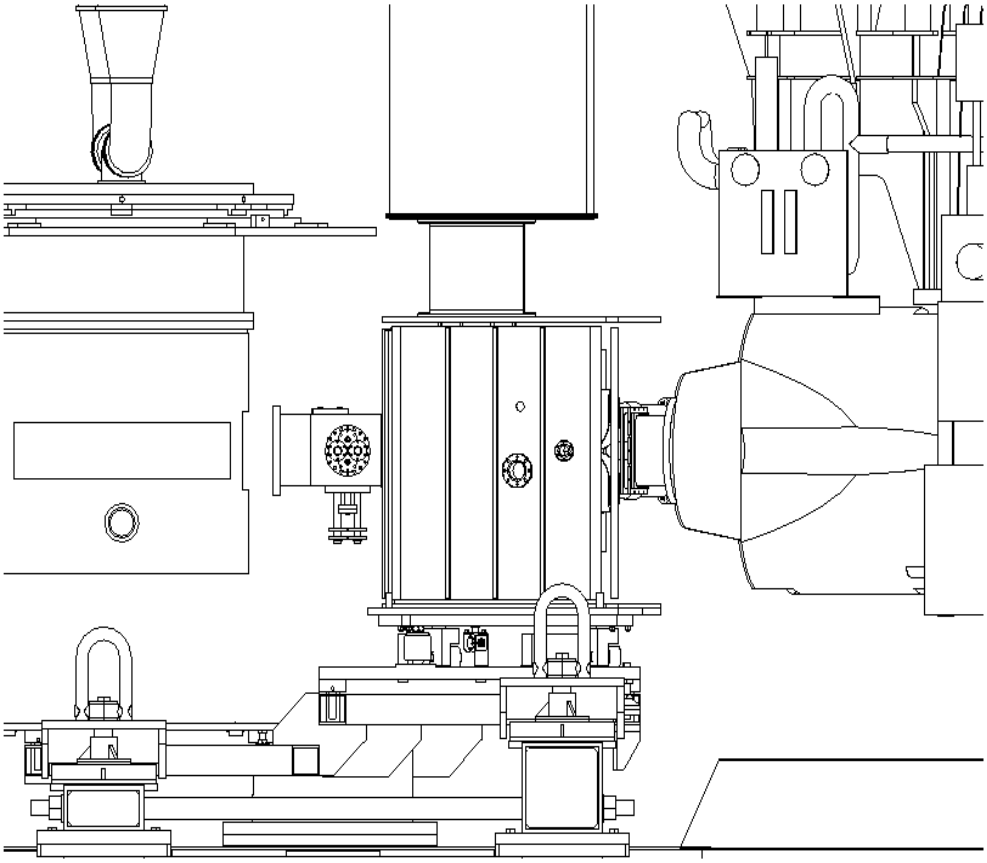

Fig. 13 The target in Hall A. Side view.

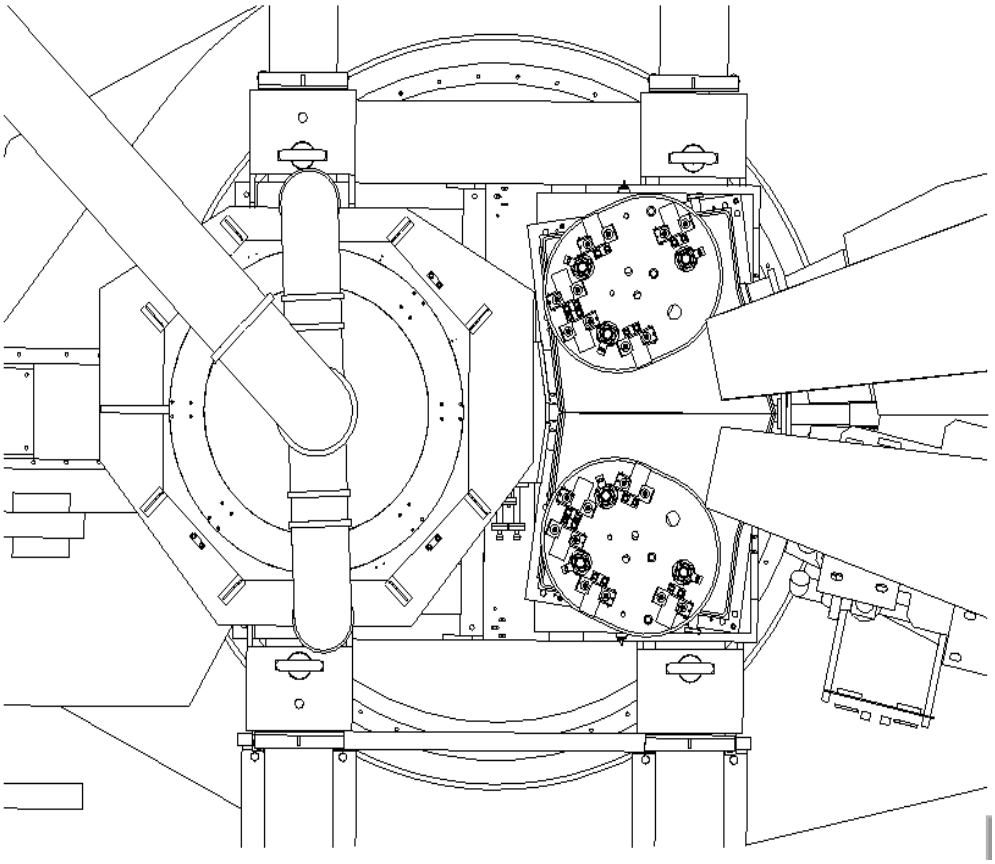

Fig. 14 The target in Hall A. Top view.

6 Proposed measurement

6.1 Kinematics

We propose a similar kinematics coverage as experiment E97-110. The HRS angle settings will be 6^o and 9^o and 6 energies will be used (1, 1.6, 2, 3, 4 and 5 GeV). The energy of the detected electrons will span from the pion threshold to the point where the proton radiative tail rate is more or less equal to the inelastic rate (unless there is overlap between the 9^o data and the 6^o ones. In this case, the 9^o are not taken). In this condition, the error on g_1 due to the radiative tail will be at worst on the order of 5%. Integrated over ν in order to get GDH, this error will become negligible.

6.1.1 Kinematics coverage

The kinematics coverage can be seen in Fig. 15. The points represent the kinematics at the acceptance centre (6^o and 9^o). Accounting for the acceptance of the septum magnets, the angular coverage will be from 4.3^o to 7.7^o and 7.3^o to 10.7^o. This will allow the formation of the integral over the $0.015<Q^2<0.4$ GeV^2 range.

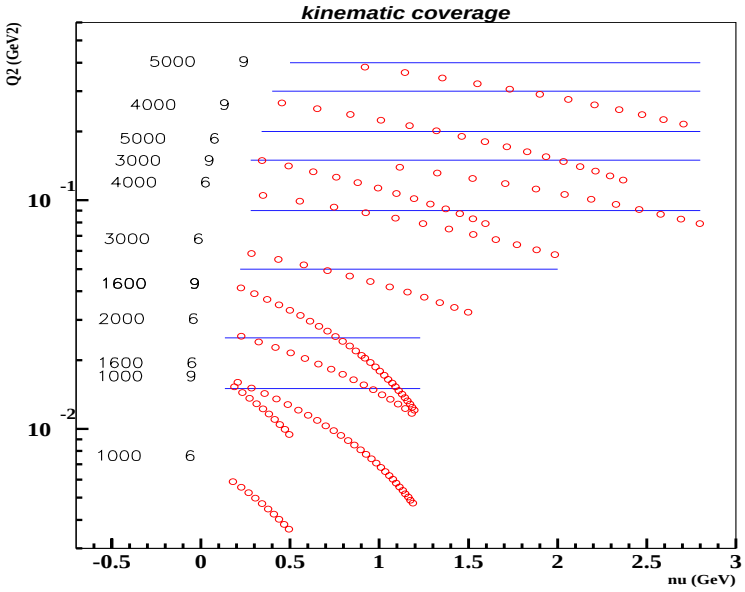

Fig. 15. Kinematics coverage. The first number is the beam energy in MeV and the second is the spectrometer angle. Each point represents the middle of the acceptance for a HRS momentum setting. The data will be interpolated in order to compute the integral at fixed Q^2. These Q^2 values and integration ranges are given by the straight lines. The data at a beam energy of 1000 MeV are for radiative corrections only.

The lowest Q^2 point at which we can reasonably integrate over ν is Q^2=0.015 GeV^2.

6.1.2 Comparison with existing data.

As said, the kinematics of the proposed experiment link the real photon line to the kinematics of the low Q^2 data from Hall B and SLAC. The coverage is shown on the figure below.

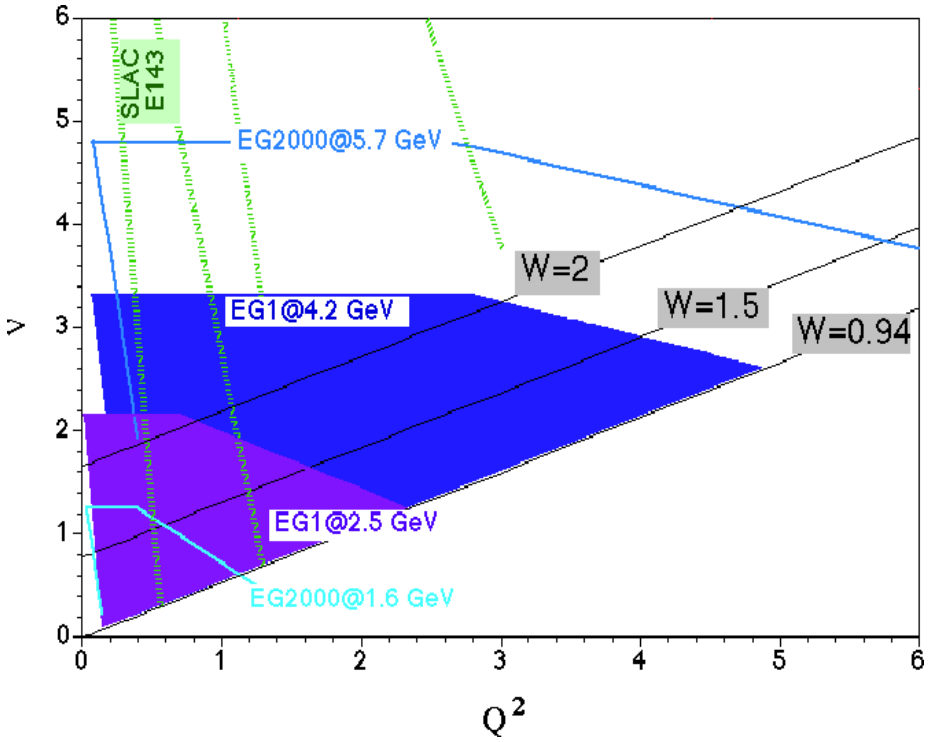

Fig. 16. Kinematics coverage of existing proton data at low Q^2 (Hall B and SLAC E143).

The lower limit of the angular acceptance of CLAS is 8^o. The acceptance becomes significant above 10^o. This is to compare with the 4.3^o lower limit of the Hall A septum magnets. For Hall B, the lowest range of integration is 0.05 GeV^2. The integration has to include the Δ resonance and account for the fact that statistics and normalization of absolute quantities on the edge of the acceptance are limited. Furthermore the Clas Cerenkov detectors are not designed for the outbending field configuration necessary to reach such low angles. These issues forbid any absolute measurement of cross sections at forward angle and $I(Q^2)$ has to be formed using asymmetry data and models for unpolarized structure functions. This adds a significant systematic that makes Clas, in its present design, not suitable for the precise measurement needed to achieve our physics goal.

Hence, the proposed experiment will be able to measure precisely $I(Q^2)$ at a significantly lower Q^2 value. Our higher Q^2 data will provide a valuable cross check of the Hall B data with an improved systematic uncertainty in the important region of the zero crossing of $I(Q^2)$.

6.2 Extraction of the data

We will measure the 2 absolute cross sections $\sigma^{\uparrow\Uparrow}$, $\sigma^{\downarrow\Uparrow}$ where $\Uparrow$ is the target spin orientation and $\uparrow$ the electron spin. From these cross sections and a model

of g_2, we can extract g_1

$$\frac{d^3\sigma^{\uparrow\Uparrow}}{d\Omega dE'} - \frac{d^3\sigma^{\downarrow\Uparrow}}{d\Omega dE'} = \frac{4\alpha^2 E'}{Q^2 E}\left[\frac{g_1}{\nu}(E + E' cos\theta) - Q^2\frac{g_2}{\nu^2}\right]$$

As stated before, the model dependence of the physics results will be small. It should be noted that the use of absolute cross section differences is a robust way of extracting g_1 because the unwanted unpolarized contribution cancels out. This extraction technique meets its full interest with the NH_3 target where the amount of extra material is large.

6.3 Rates and beam time estimate

We estimate the inelastic rates using the code QFS [33] and the following values:

- The cell length is 0.5, 1 or 3 cm
- The packing factor of the target material is 60%
- The maximal beam current is 100 nA
- The septum magnet solid angle is 4.2 msr
- The HRS momentum bite is 8%

The plots of the rates are shown in section 8. Only the single electron rates are shown. The pion rates are negligible in comparison to the electron rates.

We estimate the running time for a 0.07% (absolute)[2] error on the physics longitudinal asymmetry, a 50 MeV bin in ν, an 80% beam polarization and an 80% target polarization (average polarization achieved during the E155 experiment).

The total rate includes the proton, ^{15}N, Be windows and Liquid ^{4}He inelastic rates as well as the rates from the elastic tails. We constraint our maximal DAQ rate to 3 kHz for each HRS. For practical reasons, we required a minimum run time per HRS setting of 15 min.

The table below summarizes the results. The overhead time for each energy comes from:

- HRS momentum setting switch (30 min per setting change. In average the momentum change is in order of 100 MeV).
- Moller measurement (3 hours per energy).
- NMR calibration by thermal equilibrium measurement (2h. This will be done during other overhead times)

[2] We can assume a physics asymmetry of 1%. Typical asymmetries for the GDH experiment E94-010 at the Δ peak were 2 to 3%. We expect a decrease of the asymmetry due to Q^2 dependence.

- Dilution measurement (10 min to switch target + 10 min run each 2 HRS settings).
- Annealing (2 annealings per day: 2 hours per day).
- The time for switching from one cell to another is negligible (10 min) and will be done during the HRS setting change.

E GeV	θ	ν range GeV	cell length	Beam time (1 HRS)	Overhead	Total (2 HRS)
$1.0^{(1)}$	6^o	0.156-0.500	0.5 cm	11.0 hours	7.2	12.3
1.6	6^o	0.165-1.200	0.5 cm	69.9 hours	18.15	50.2
2.0	6^o	0.173-1.200	0.5 cm	39.7 hours	12.3	30.5
3.0	6^o	0.202-1.500	3 cm	14.4 hours	8.9	15.5
4.0	6^o	$0.241^{(2)}$-2.000	3 cm	17.45 hours	9.1	17.1
5.0	6^o	$1.000^{(2)}$-2.800	3 cm	34.2 hours	10.5	26.2
1.0	9^o	0.163-0.500	0.5 cm	23.3 hours	8.3	19.0
$1.6^{(1)}$	9^o	0.183-0.920	1 cm	43.5 hours	12.0	31.9
1.6	9^o	0.900-1.200	0.5 cm	59.2hours	12.0	39.1
3.0	9^o	0.264-1.600	3 cm	86.7 hours	15.6	55.3
4.0	9^o	$0.350^{(2)}$-2.400	3 cm	81.2 hours	11.3	48.5
5.0	9^o	$0.800^{(2)}$-2.800	3 cm	85.0 hours	11.0	50.1

(1) For radiative corrections only. The statistical uncertainty on the raw asymmetry is taken to be 0.1% instead of 0.07%.

(2) For such a setting, only the left HRS can be used because of the limitation of the right HRS. In this case, part of the data taking will be not performed in a symmetric way as for the rest of the experiment: The left HRS will take the high E' data while the right one will take lower E' data.

In addition we have counted:

- One absolute beam energy measurement each energy (2 hours per energy, total of 22 hours).
- Energy change (8 hours for a linac change and 4 for a pass change. Total of 48 hours).
- Septum angle switch (16 hours).

The total time for the experiment is 481 hours (20 days).

6.4 Statistical and systematic uncertainties

The uncertainty on the integral is dominated by the systematics, the statistical error being reduced by the integration over ν. The statistical error on the integral, including the contribution from the unpolarized materials, will be 1 to 2%. The error on non-integrated quantities such as g_1 will be typically 6% for a 150 MeV bin.

We can reasonably assume an error of 3% on both beam and target polarimetries. The systematic uncertainty on the absolute cross section will be at the 5% level. Another 3% will come from the interpolation needed to integrate g_1 at fixed Q^2 (see fig. 15). The use of a model for g_2 will introduce a systematic uncertainty of 2 to 3%. It will make a total of 8% systematic error except at large ν where the systematic uncertainty due to the elastic tail subtraction will become sizeable. We should note that most of the systematic errors will have been understood after the experimental run of the low Q^2 GDH experiment E97-110.

7 Summary

In summary, we propose to measure the extended GDH integral on the proton in the range $0.015<Q^2<0.4$ GeV^2. This range is reachable with a beam energy spanning from 1.6 GeV to 5 GeV and with the septum magnets that provide an angular coverage from 4.3^o to 10.7^o. The Q^2 coverage and expected systematic uncertainties are shown in the figure below. Also shown is how the proposal is completing the data taken during the CLAS experiment EG1a [22].

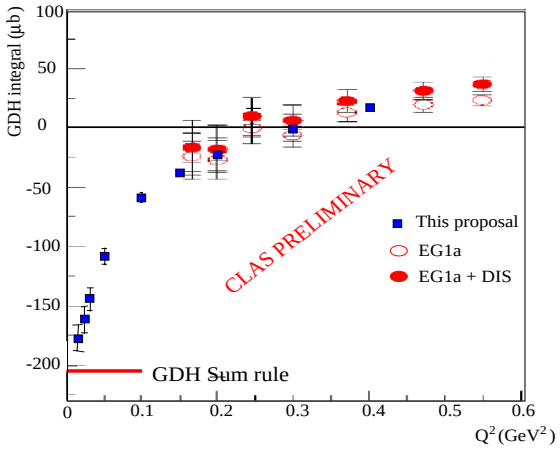

Fig. 17. Coverage and expected systematic uncertainties for this proposal. The experimental data points are preliminary data from EG1a. The positions of the expected data points are simply estimated assuming a smooth transition between the EG1a data and the GDH sum rule at Q^2=0.

Such a measurement by itself will:

- Complete the world data on the Q^2 evolution of the proton extended GDH integral by providing the missing part at low Q^2.
- Provide a benchmark measurement for χPT without the additional uncertainty of nuclear effects coming with the nucleon extraction.

The extrapolation to Q^2=0 can be done using models or calculations if these are validated by our data. If not, a linear extrapolation after the turn over should be sufficient given the value of the loweest Q^2 point. After extrapolation to Q^2=0, it will:

- Provide a check of the original GDH sum rule on the proton using a technique differing from the one currently used at MAMI/ELSA and JLAB Hall B.

Together with the E97-110 neutron data available soon from Hall A, it will:

- Provide a measurement of the evolution of the "Bjorken" integral at low Q^2. This quantity is ideal to link the domain where χPT is applicable to the domain calculable with the Operator Product Expansion technique. For this purpose, the "Bjorken" integral is a better quantity than the GDH integral because the complication due to the resonances mostly cancels out.

- Verify the "Bjorken" sum rule at the photon point, this quantity being predicted by the nucleon GDH sum rules. The extrapolation to the photon point is facilitated by the expected smoothness of the Q^2 evolution of the Bjorken integral.

The proton data, neutron data and their difference will help to disentangle issues with χPT calculations. The Isoscalar, Isovector and interference GDH sum rules at the photon point can also be formed.

In addition to the standard Hall A equipment, the experiment requires the use of the Hall A septum magnets, the UVa/Hall C/SLAC NH_3 polarized target and the CEBAF polarized beam.

With 20 days of beam time, the uncertainty on the GDH integral will typically be $\pm$2% (stat) $\pm$8% (syst). The error on the spin structure function g_1 will be $\pm$6% (stat) $\pm$8% (syst) for a 150 MeV bin in ν.

8 Appendix: Plots of the rates

The plots of the rates are given here in the conditions of section 6.3. For the background, the inelastic proton rate has to be compared only to the elastic proton tail. The nitrogen contribution cancels out. However, since the nitrogen rate is a limiting factor because it saturates the DAQ maximal rate, it is plotted as well.

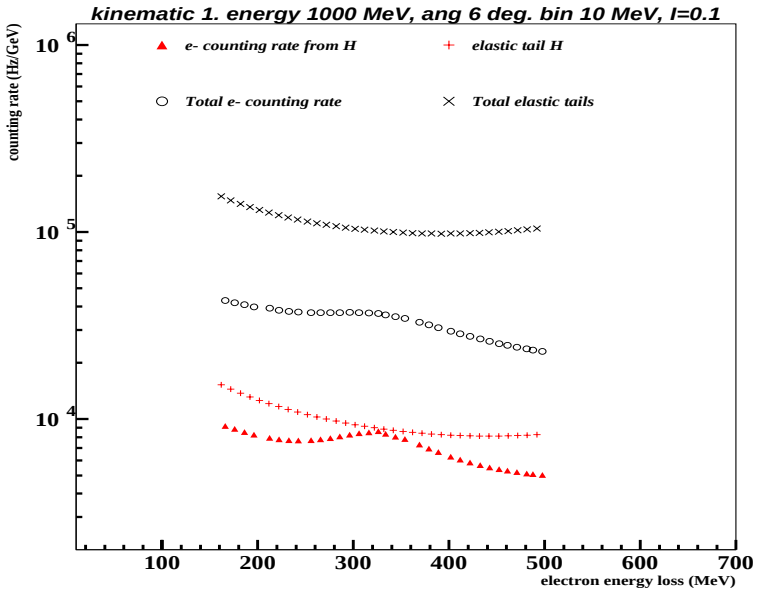

Fig A1. Kinematic 1. The triangle and + symbols give the rate from the hydrogen. The total rate (NH_3 + He + Be) is given by the circle and the × symbols.

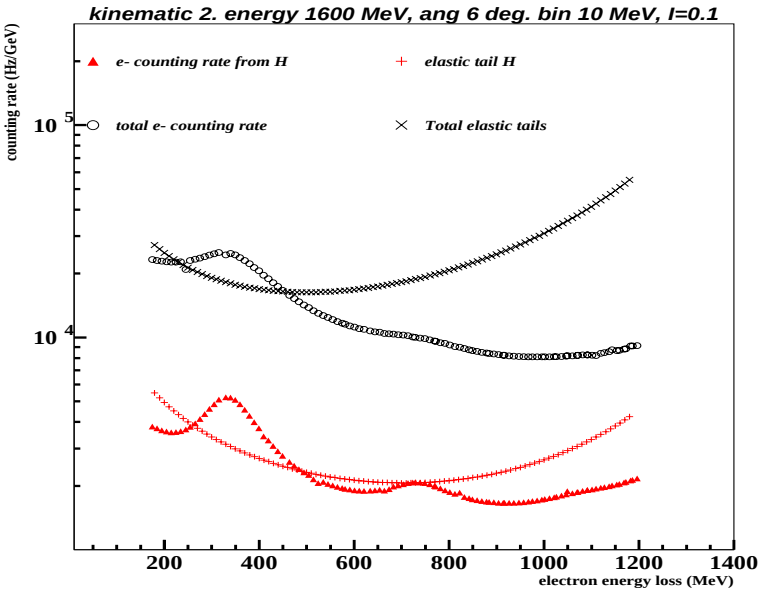

Fig A2. Kinematic 2

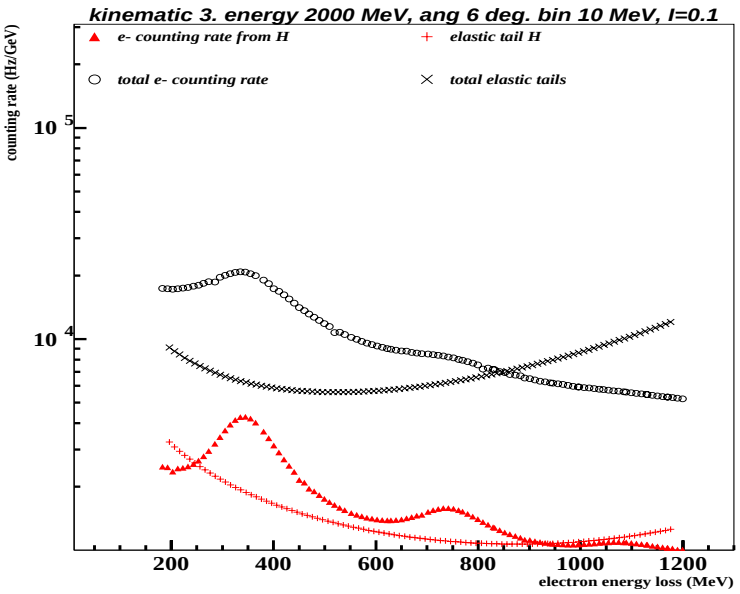

Fig A3. Kinematic 3

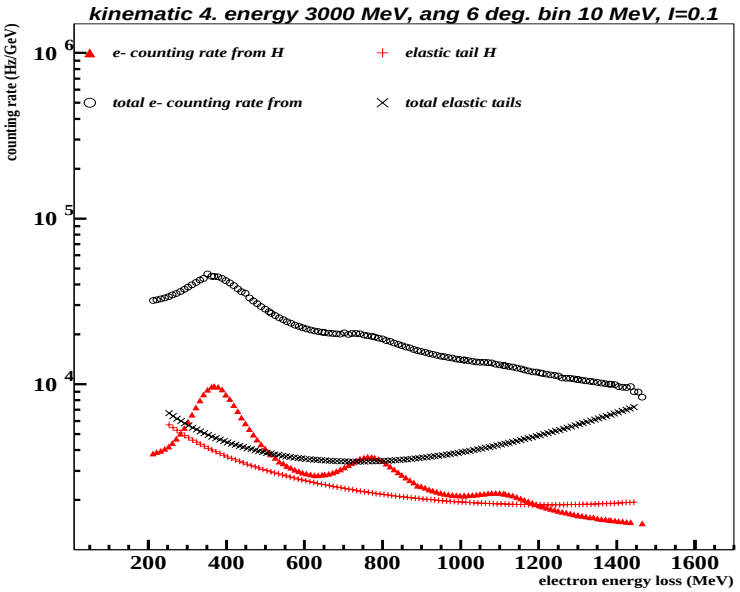

Fig A4. Kinematic 4

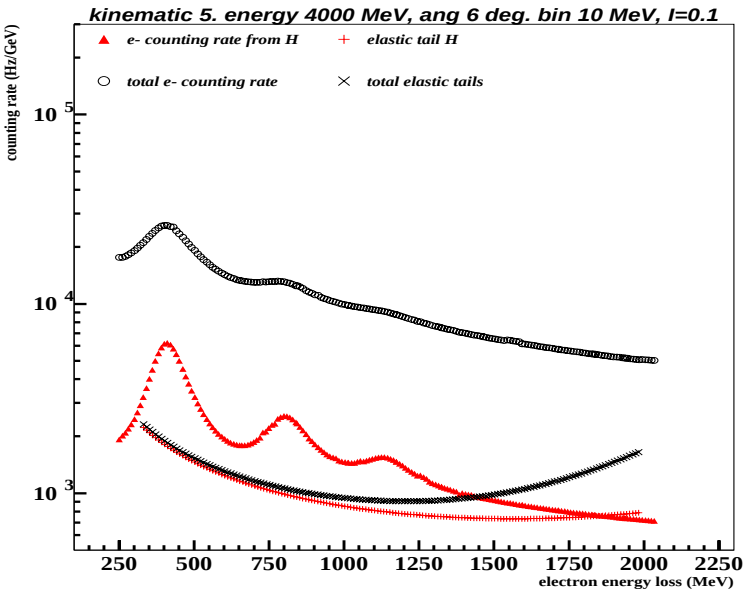

Fig A5. Kinematic 5

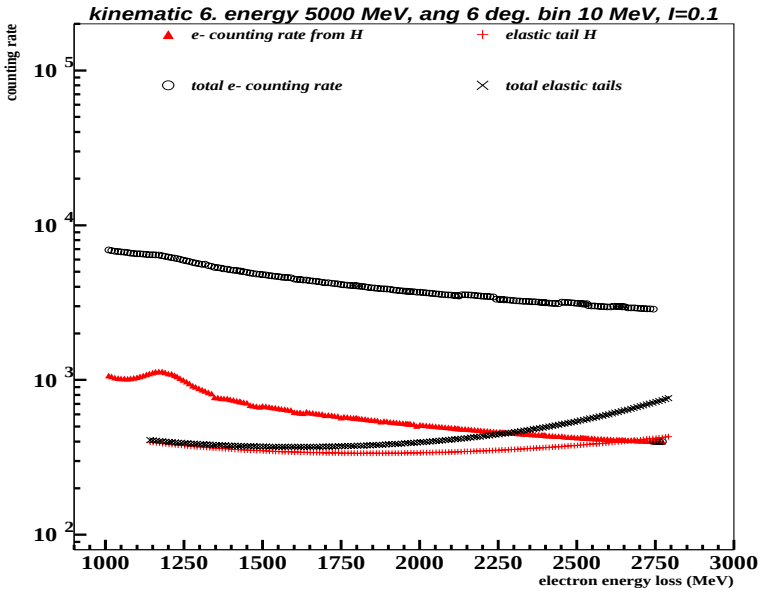

Fig A6. Kinematic 6

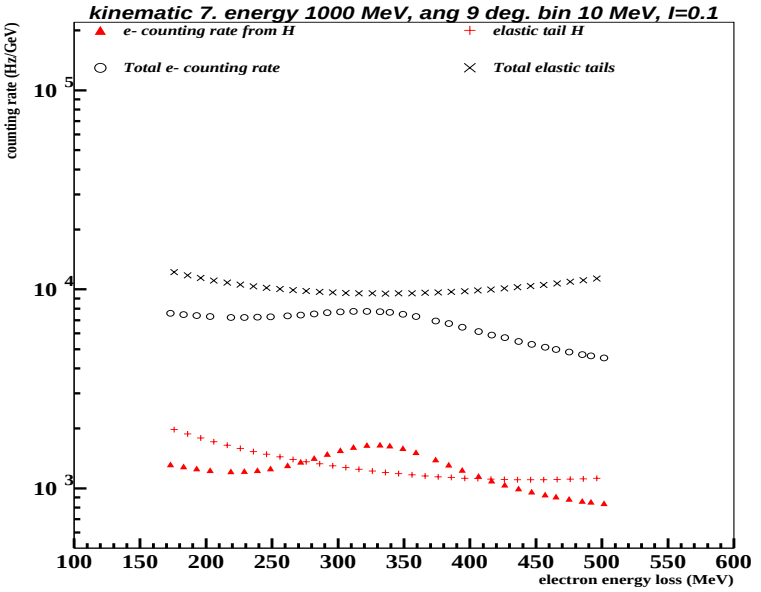

Fig A7. Kinematic 7

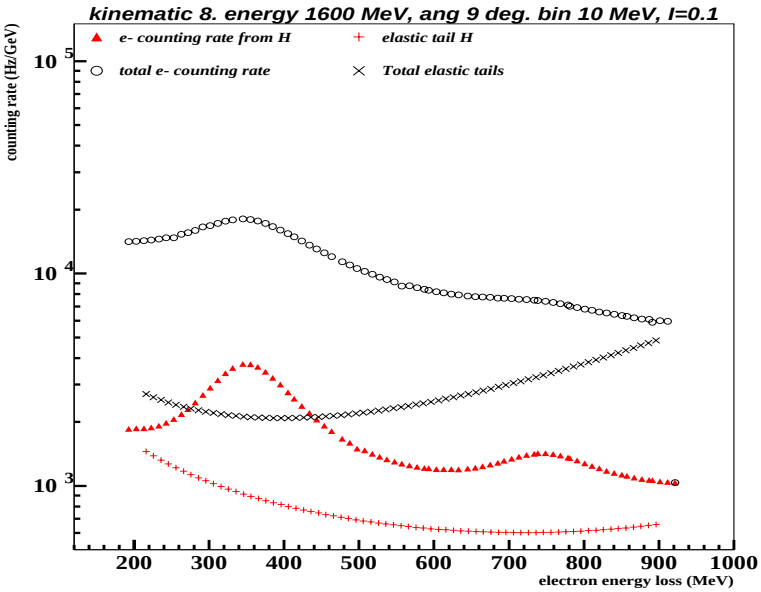

Fig A8. Kinematic 8

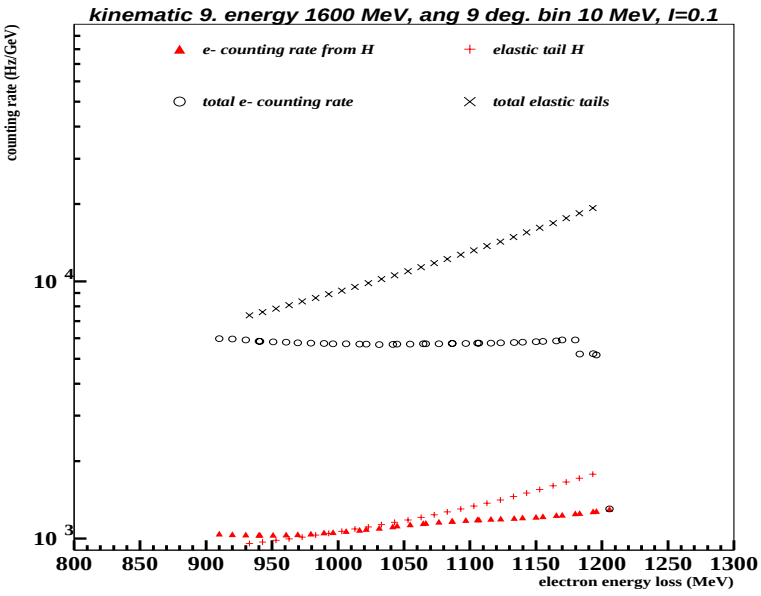

Fig A9. Kinematic 9

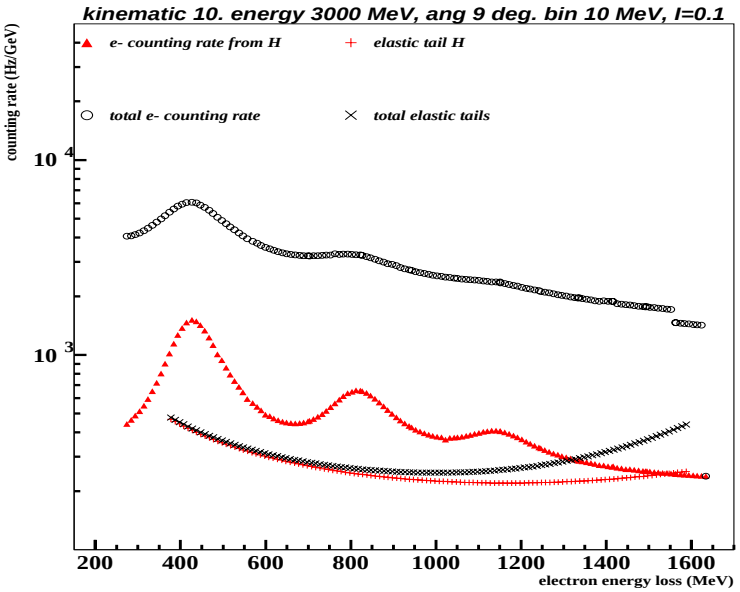

Fig A10. Kinematic 10

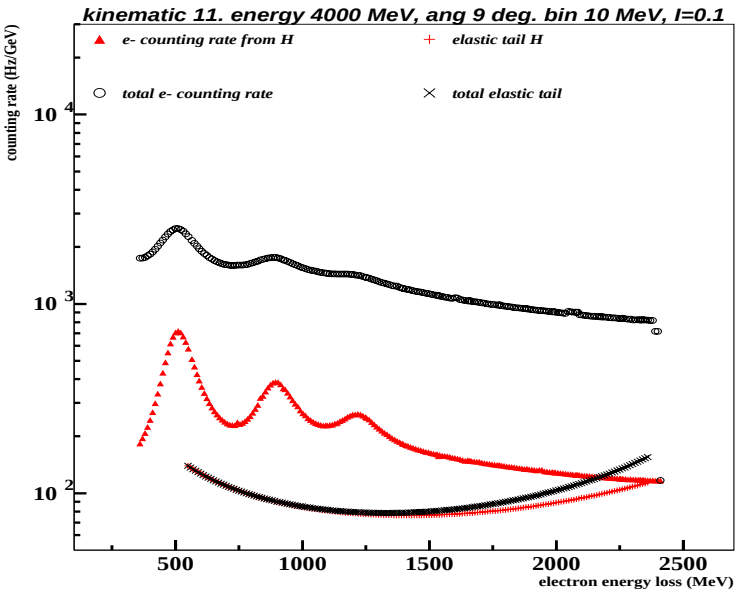

Fig A11. Kinematic 11

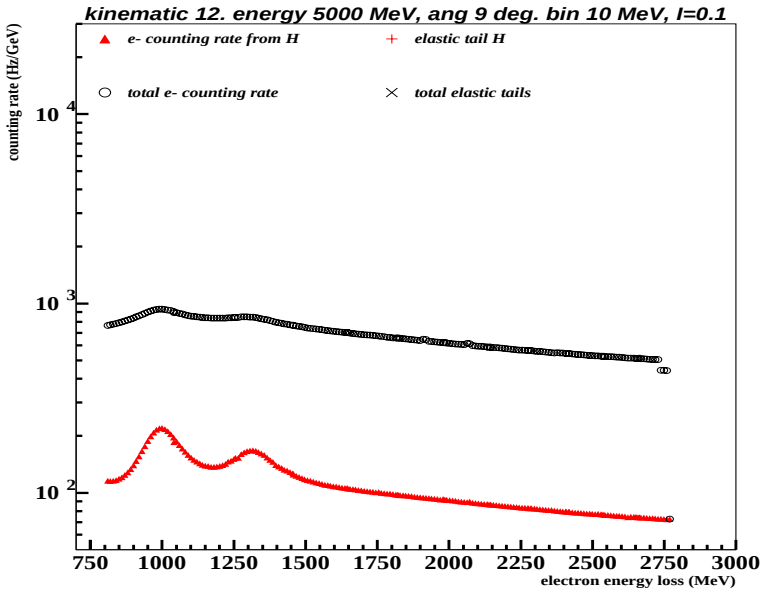

Fig A12. Kinematic 12

References

[1] S. Gerasimov. Yad. Fiz. 2 598 (1965). S. D. Drell and A. C. Hearn. Phys. Rev. Lett. 16 908 (1966).

[2] S. Bass. Z. Phys. A. 355. 77 (1996)

[3] I. Karliner. Phys. Rev D. 7. 9 (1973). Workman and Arndt. Phys. Rev. D45 1789 (1992).

[4] Ahrens *et al.* Phys. Rev. Lett. 87, 22003 (2001)

[5] http://wwwa2.kph.uni-mainz.de/publications/

[6] K. Helbing. Talk given at the Spin2002 conference. http://www.c-ad.bnl.gov/SPIN2002/presentations/Helbing.pdf

[7] http://isnwww.in2p3.fr/graal/graal_anglais.html

[8] http://www.legs.bnl.gov/

[9] SLAC proposal E-159. P.E Bosted and D. Crabb spokespersons.

[10] http://www.spring8.or.jp/

[11] http://www.tunl.duke.edu/~capture/

[12] M. Anselmino, B.L. Ioffe and E. Leader, Sov. J. Nucl. Phys. 49, 136, (1989).

[13] D. Drechsel et al. Phys. rev. D63 114010 (2001).

[14] X. Ji and J. Osborn. J. Phys G27 127 (2001).

[15] SMC collaboration. Phys. Rev. D58 112001 (1998)

[16] E143 collaboration. Phys. Rev. Lett. 78. 815. (1997)

[17] HERMES collaboration. Phys. Lett. B444 531 (1998).

[18] V. Bernard, N. Kaiser, U-G. Meiβner. Phys.Rev. D48 (1993) 3062-3069 ; V. Bernard, T. R. Hemmert, U-G. Meiβner. hep-ph/0203167 (2002)

[19] X. Ji, J. Osborne. J.Phys. G27 (2001) 127 ; X. Ji, C-W Kao, J. Osborne. Phys.Rev. D61 (2000) 074003

[20] GDH2002 workshop. Genova 2002.

[21] Amarian *et al.* (the GDH E94010 collaboration). Submitted to Phys. Rev. Lett. Nucl-ex/0205020

[22] http://www.jlab.org/~kuhn/EG1intro.html

[23] JLab E97-110. J.P. Chen, A. Deur and F. Garibaldi spokespersons.

[24] V. D. Burkert, Phys. Rev. D 63, 097904 (2001).

[25] I. Karliner. Phys. Rev. D. Vol 7 9 (1973).

[26] S. Bass Mod.Phys.Lett. A12 (1997) 1051-1068

[27] JLAB E01-104. D. Crabb, M. Khandaker, D. Sober spokepersons.

[28] H. Arenhoevel GDH2000 proceedings, D.Drechsel and L. Tiator Pub. World Scientific (2001), and personal communication.

[29] D. Drechsel, S.S. Kamalov, L. Tiator. Phys.Rev. D63 (2001) 114010

[30] V. Burkert and Z. Li. Phys. Rev. D 47 46 1993.

[31] Y. Roblin, roblin@jlab.org. Personal Communication.

[32] Hall A 12 GeV Upgrade. Conceptual design (September 8, 2002) p27.

[33] Lightbody and O'Connell. Computer in Physics, May/June 1988